

Data Analysis and Modeling With a Hybrid Detector

Daniel Yankura

A senior thesis submitted to the faculty of
Brigham Young University
in partial fulfillment of the requirements for the degree of
Bachelor of Science

John E. Ellsworth, Advisor

Department of Physics and Astronomy
Brigham Young University

Copyright © 2023 Daniel Yankura

All Rights Reserved

ABSTRACT

Data Analysis and Modeling With a Hybrid Detector

Daniel Yankura

Department of Physics and Astronomy, BYU

Bachelor of Science

The goal of this research is to support the project to quantify electrons observed from nuclear fusion reactions. For the first part of this project we developed code in MATLAB to interpret data collected by a hybrid detector. This detector has a silicon wafer in front to discriminate against gamma rays, followed by a block of polyvinyl toluene (PVT) where the electrons are stopped, and the energy they deposited is recorded. It was tested using Cs 137, and the detector was able to resolve the energy of the Cs conversion electrons. For the second part of this project we created a model of the detector using Geant4 Monte Carlo particle simulation toolkit. After verifying that our model matched our detector's output for low energy electrons, we ran simulations in the multi-MeV range. This allowed us to predict its behavior with higher energy electrons. We report that this hybrid detector is able to effectively detect electrons in the 0.5 MeV range. Furthermore, our current simulations report that our detection system is likely to remain effective for electrons in the multi-MeV range.

Keywords: Monte Carlo, Geant4, Electron Spectroscopy, Fusion, Polyvinyl Toluene, Conversion Electrons

ACKNOWLEDGMENTS

First and foremost I would like to thank my advisor John Ellsworth. He has taught a great deal about nuclear physics, detector design, and has helped me develop a number of skills. I am grateful for all the time that he dedicated to helping me with my research, and for all the guidance that he gave along the way. I would also like to thank my family and friends who have supported me throughout the various challenges of my academic career. Lastly, I would like to acknowledge the support and funding I received from Brigham Young University's College of Physical and Mathematical Sciences.

Contents

Table of Contents	vii
List of Figures	ix
1 Introduction	1
1.1 Motivation	1
1.2 Overview of Nuclear Fusion	2
1.3 Overview of Electron Screening	3
1.4 Detector Overview	4
1.5 Research Overview	6
2 Methods	9
2.1 Data Collection	9
2.2 Post-Processing of Data	10
2.3 Geant4	14
3 Results & Conclusions	23
4 Future Work	25
Appendix A Appendix Title	27
A.1 Electron Spectrum Code	27
A.2 Geant4 Macro File	29
A.3 Geant4 Geometry File	32
A.4 Geant4 PVT File	34
A.5 Root Commands	34
A.6 Sellmeier Code	35
Bibliography	37
Index	39

List of Figures

1.1	Plot of Coulomb Barrier	4
1.2	Top View of Detector	5
2.1	Electron Event Example	11
2.2	Cs137 Spectrum	12
2.3	Sr90 Spectrum	13
2.4	Index of Refraction Vs Wavelength for PVT	15
2.5	Simulated electron spectrum for PVT	17
2.6	Simulation of Photon Energies	18
2.7	Detector Simulation With High Energy Electrons	19
2.8	Electron Spectrum Plot for High Energy Electrons	20
2.9	Energies Passing through PVT	21
A.1	Electron Spectroscopy Code Part 1	27
A.2	Electron Spectroscopy Code Part 2	28
A.3	Electron Spectroscopy Code Part 3	29
A.4	Macro File Part 1	30
A.5	Macro File Part 2	31
A.6	Geometry File Part 1	32

A.7	Geometry File Part 2	33
A.8	Geant4 file with optical data used in simulation of PVT	34
A.9	Sellmeier Equation Code	35

Chapter 1

Introduction

1.1 Motivation

Over 100 years ago, Sir Arthur Eddington correctly theorized that the Sun's energy came from nuclear fusion reactions. Since then our understanding of nuclear fusion has advanced significantly. In the past decade alone, billions of dollars have been spent on research into harnessing fusion as a source of energy. Advances have been allowing for increasingly efficient fusion reactions to be produced in laboratory experiments. Recently, the first net positive fusion reaction was achieved at Lawrence Livermore National lab. Despite this, the physics behind fusion is not entirely understood, and there remain a number of questions that still need answering.

One discrepancy that has arisen is between experimental and theoretical fusion rates. In lower energy fusion reactions, experimental fusion rates have exceeded theoretical predictions by as much as a factor of two [1]. The end goal of our research is to experimentally test theories that aim to resolve this issue. To do this, we first need detectors that can accurately collect data from the byproducts of fusion reactions. As part of our research, we verified the efficacy of our ΔE -E electron detector in the 0.5 MeV range, and then used Geant4 particle simulation software to predict detector

behavior in the multi-MeV range.

1.2 Overview of Nuclear Fusion

In nuclear fusion, there are two main forces at work. The first is a repulsive force between two atomic nuclei because of their positive charge. The second is the strong nuclear force which attracts all atomic nucleons (protons and neutrons). The strong nuclear force is much stronger than the repulsive coulomb force, but is only effective over much smaller distances.

Fusion occurs when two atomic nuclei have enough energy that they can overcome the repulsive force, known as the Coulomb barrier, and get close enough that the strong nuclear force takes over and binds them together. When two nuclei bind, they release energy usually in the form of electromagnetic radiation, neutrons, and other heavy charged particles (protons, tritons, helions (He-3), and alphas). It is this process which powers all stars and which will hopefully be a source of energy for humanity in the future.

Aside from the Coulomb repulsive force, and the strong nuclear force, there are other physical processes which affect the fusion reaction. One such process is quantum tunneling. From quantum mechanics we know that particles behave not as well defined points of charge, but as probabilistic wave functions. In the case of a particle interacting with a finite barrier, it is possible for the wave function to exist on the other side of the barrier, making it possible for it to be observed on the other side, even if it lacks the energy to overcome it.

Since the coulomb barrier is a finite barrier, we know that there is a possibility of a nuclei tunneling through this barrier. This means that even if our nuclei do not have enough energy to overcome the coulomb barrier, that fusion is still possible. Given enough atoms of a certain energy in a confined environment, we can therefore predict what percentage of them will tunnel and undergo fusion. The lower the barrier is, the greater the chance there is of tunneling.

1.3 Overview of Electron Screening

Electrons also play an important role in fusion reactions. Since electrons have an equal and opposite charge to that of protons they can effectively reduce the coulomb barrier. Outside of an electron cloud, the coulomb potential is reduced to zero, and even inside the cloud the potential is reduced. The screening effect of electrons on the nucleus increases fusion rate by lowering the energy threshold at which fusion can occur. As the Coulomb barrier is lowered, tunneling rates would increase as well.

The effect of electrons on the Coulomb barrier is shown in Fig. 1.1. The dashed line shows the Coulomb Barrier with no electrons present. The solid line is the Coulomb barrier when electrons are present. As shown, the potential is reduced at all points, and is zero outside of the electron cloud where the net charge of the atom is now zero. At any point along the potential quantum tunneling is possible. However, as the energy of an incoming particle increases, so does its chance of tunneling. The reduced potential from electrons also increases the probability of tunneling.

However, there are still a number of unanswered questions. Laboratory experiments with accelerators have yielded fusion rates higher than theoretical expectations, with experimental rate sometimes being twice as high as theoretical [2–4]. This implies that there is another factor at play that is lowering the coulomb barrier even more.

The prevailing theory is that electrons play an even larger role in fusion than previously theorized. The discrepancy between experimental and theoretical rates could be explained if the electron was somehow closer to the nucleus. The Bohr model of the atom predicts that electrons can only exist in specific orbitals. The radius of these orbitals are determined by the charge and mass of the nucleus and the electron in the orbital. Quantum mechanics however would allow for the electron to exist closer. If an electron were to get caught in the potential well formed by two approaching nuclei, it could get closer to the nucleus than it would be in the lowest orbital possible. This would lower the Coulomb barrier even further than electron screening normally would. [5]

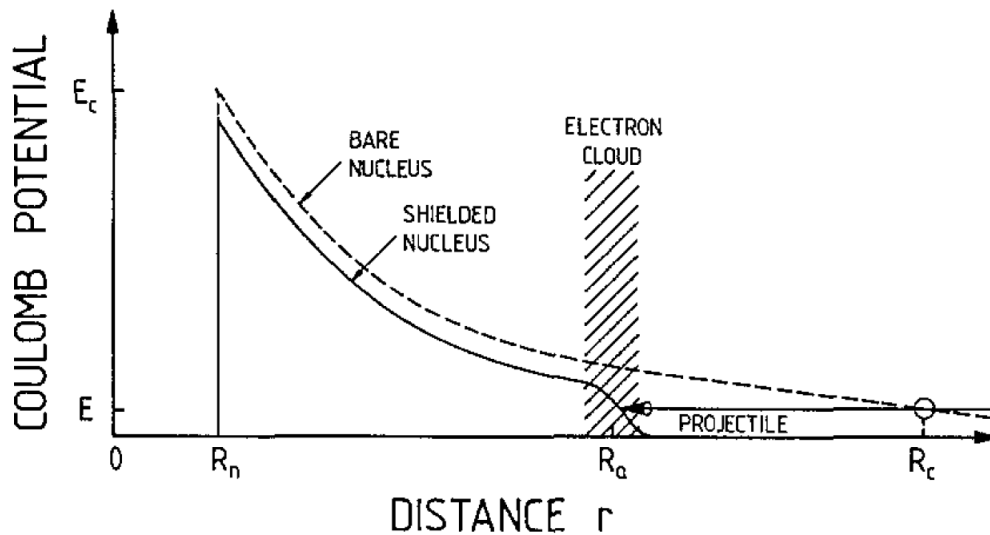


Figure 1.1 Diagram of Coulomb barrier borrowed from Rolfs's *Cauldrons of the Cosmos* [6]. When two nuclei approach each other, the repulsive force increases. As shown, the presence of electrons reduces the Coulomb barrier, thereby reducing the energy needed for fusion to occur.

1.4 Detector Overview

Since we can not observe fusion reactions directly we can only learn about them by observing their byproducts. Fusion reactions can result in the release of gamma rays, neutrons, and even electrons. Previous students in the Laboratory Nuclear Astrophysics Research group (LNAR) helped design and build a ΔE - E detector for heavy particle energy spectroscopy. It could effectively discriminate energetic protons, tritons, helions, and alphas. However, it was ineffective at detecting electrons because the ΔE - E detectors were too thin to recognize an electron above the background noise. Furthermore, this stop detector would not have been large enough to stop multi MeV electrons. This detector design was modified however, as part of our experiments, to work effectively as an electron detector. A top-view picture of our detector is included below in Fig. 1.2.

The new ΔE - E detector has three main components to it: a thin silicon wafer, a block of polyvinyl toluene (PVT), and four photo-multiplier tubes (PMTs). At the end of the detector is

the block of PVT. The PVT is what stops the particles, and scintillates, producing visible light [7]. At one end of the block are the four PMTs. The light produced from the PVT is picked up and measured by the PMTs. Measuring the energy of the light allows us to deduce the energy of the electron stopped by the PVT.

However, the PVT is also highly effective at detecting gamma rays, which can be emitted by a number of outside sources including building materials and cosmic rays. To filter out this background noise we placed a thin silicon wafer in front of our PVT. This wafer is sensitive to electrons, but not gamma rays. When a particle deposits energy on the silicon wafer it signals our system to start recording, allowing us to record data from the electron event, while filtering out unwanted noise from background radiation.

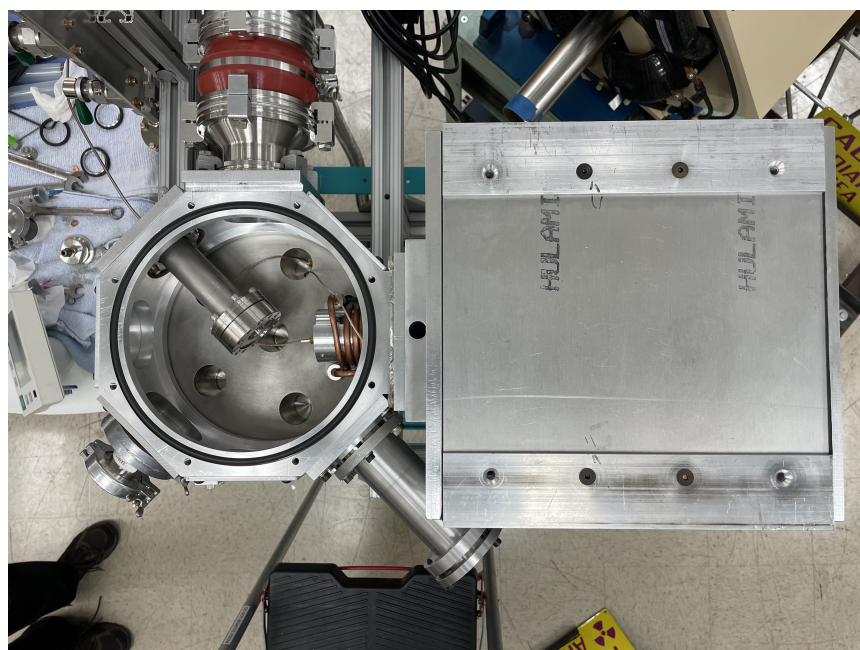


Figure 1.2 A top view of the detector used. The chamber on the left was where radioactive sources could be placed. Above the chamber is a turbo-pump used to achieve a better vacuum. To the right is the metal casing that enclosed the polyvinyl toluene (PVT), with the silicon wafer being placed in the tube between the chamber and the PVT. Photo-multiplier tubes (PMTs) are built into the right side of aluminum box

1.5 Research Overview

As mentioned in our overview of electron screening, the prevailing theory is that during fusion, the probability functions of an electron, and two nuclei can overlap during fusion. This would allow the electron to get closer to the nuclei than it could in the electron cloud. In this situation, instead of emitting a gamma ray as a fusion byproduct, an electron of equivalent energy would be emitted [8]. For a fusion reaction involving a proton and deuterium, we would normally expect to observe $p + d \rightarrow 3He + \gamma$ (5.6 MeV). With this new model for electron screening we would instead see $p + d \rightarrow 3He + e^-$. However, now the electron would have 5.6 MeVs of energy minus the binding energy. The ultimate goal of our research is to detect these catalyst electrons to determine if this theory is viable or not.

Our research was divided into two parts. First, we tested our detector with two radioactive isotopes, Cs 137 and Sr 90. These sources undergo β^- decay which can emit electrons. This allowed us to ensure that the detector could in fact work with electrons. However the electrons emitted by these sources are at a much lower energy than those produced through fusion reactions. β^- decay typically produces electrons in the 0.5 MeV range. A fusion reaction between two deuterium nuclei has three possible outcomes. One of these results in a 23.5 MeV photon being emitted (the most energy for any fusion reaction). Therefore the highest energy electrons we would expect to observe would be 23.5 MeV.

In order to test our setup without procuring a high energy electron source, we made a model of our detector using Geant4's particle simulation software. We calibrated our model by comparing its output to that of our detector, and then simulated the same process but with higher energy electrons. At higher energy levels, a number of issues can occur with data collection. The main concern is detector efficiency. In the multi-MeV range, electrons may not be stopped by the PVT. If an electron passes completely through our detector, no information can be collected. Electrons that are stopped could produce gamma rays. The PVT should detect gamma rays unless they escape

our detection system early, which would result in more lost data. The lower our detector efficiency (number of electrons detected over number reaching detector), the longer it would take to collect data. By testing our model with electrons in the multi-MeV range we can predict if this will be an issue, before testing our detector with an actual source.

Chapter 2

Methods

To test our detector's capabilities, we tested it with Cesium 137 and Strontium 90. The sections below detail how data was collected and digitized using our detector setup. We also detail the post-processing methods used to create electron spectrum plots. Lastly, we created a model of our detector with Geant4 simulation software. This model enabled us to predict our detector's effectiveness with higher energy electrons.

2.1 Data Collection

There are two components of the detector that collect data. The first is the silicon wafer between the target chamber and the PVT. The silicon wafer is insensitive to gamma rays. This allows us to discriminate electrons in a strong field of gamma rays, such as those produced through β^- decay of Cs137, or those from background radiation. When an electron hits the wafer it deposits some energy without stopping entirely. This energy is converted into an electrical signal which is recorded by our digitizer. This then signals the rest of the detector to start recording. When the electron hits the PVT it is stopped, the PVT scintillates, and the subsequent light produced is measured at the other end of the block where four PMTs are placed. The data from the PMTs is then passed through the

digitizer, and recorded along with the data from the silicon wafer.

Prior to recording data, a series of steps were followed to prepare the detector. After installing the source in the detector chamber, the chamber was evacuated to a pressure in the 10^{-6} Torr range. LN2 vapor was used to cool the silicon wafer to reduce its inherent background noise. Once preparations were complete, we had to run the detector between 800 - 1100 seconds, to collect enough data to create an electron spectrum plot for our source.

2.2 Post-Processing of Data

In order to create an electron spectrum plot, the data needs to be processed. As shown in Fig. 2.1, the detector records multiple inputs from a single electron event. The top plot is the energy recorded in the silicon wafer over time. The bottom plot is a logic gate that tells when the detector started and stopped recording. The second and third plot are both the energy deposited in the PVT. The second is recorded with a low gain for higher energy electrons. The third is the same but with a high gain filter for lower energy events.

The most important of these four plots are the second and third. We wrote a script in MATLAB that went through each event, and from these two plots found the energy deposited from each event. This code can be found in Appendix A.1. False events did occur occasionally. This could happen when the energy deposited was too low to get an energy curve, or where background noise was detected in coincidence with an electron hitting the silicon wafer. These were filtered out during post-processing by our MATLAB script.

For each event, we found the energy by measuring the peak of each pulse which is proportional to the energy deposited in the PVT. Pulse height data was plotted as histograms with the abscissa representing energy, and the ordinate showing the count of pulses at a particular energy. The abscissa in the plots are plotted using arbitrary units and are not calibrated. Two of the spectrum's

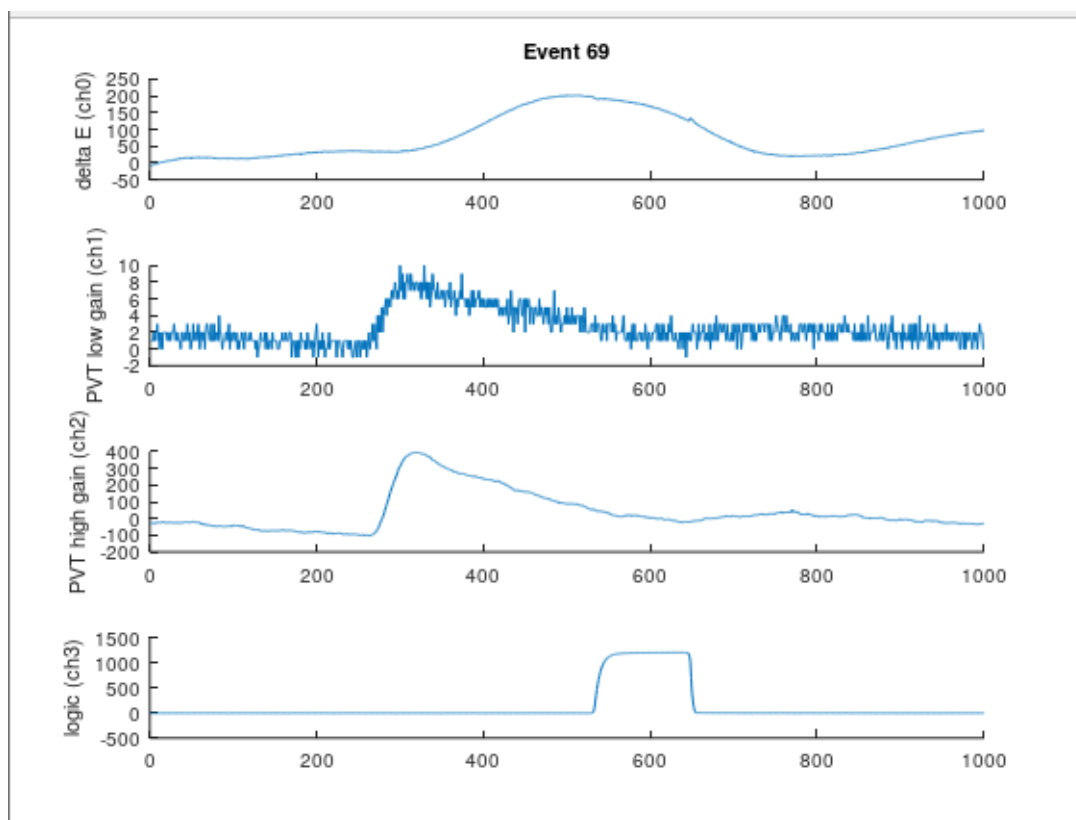


Figure 2.1 Single electron event. Top plot is the energy deposited in the silicon wafer as a function of time. The second and third are the energy deposited in the PVT. The second is recorded with a lower gain for high energy events, and the third with a high gain for lower energy events. The fourth plot is a logic pulse that indicates a waveform was recorded.

we produced are shown below in Figs. 2.2 and 2.3. These isotopes have been very well studied, and electron spectrum plots of them are readily available. By comparing ours to known sources, we have verified that our detector can achieve high enough resolution to detect the features of an electron's spectrum.

Electron Spectrum for Cs137

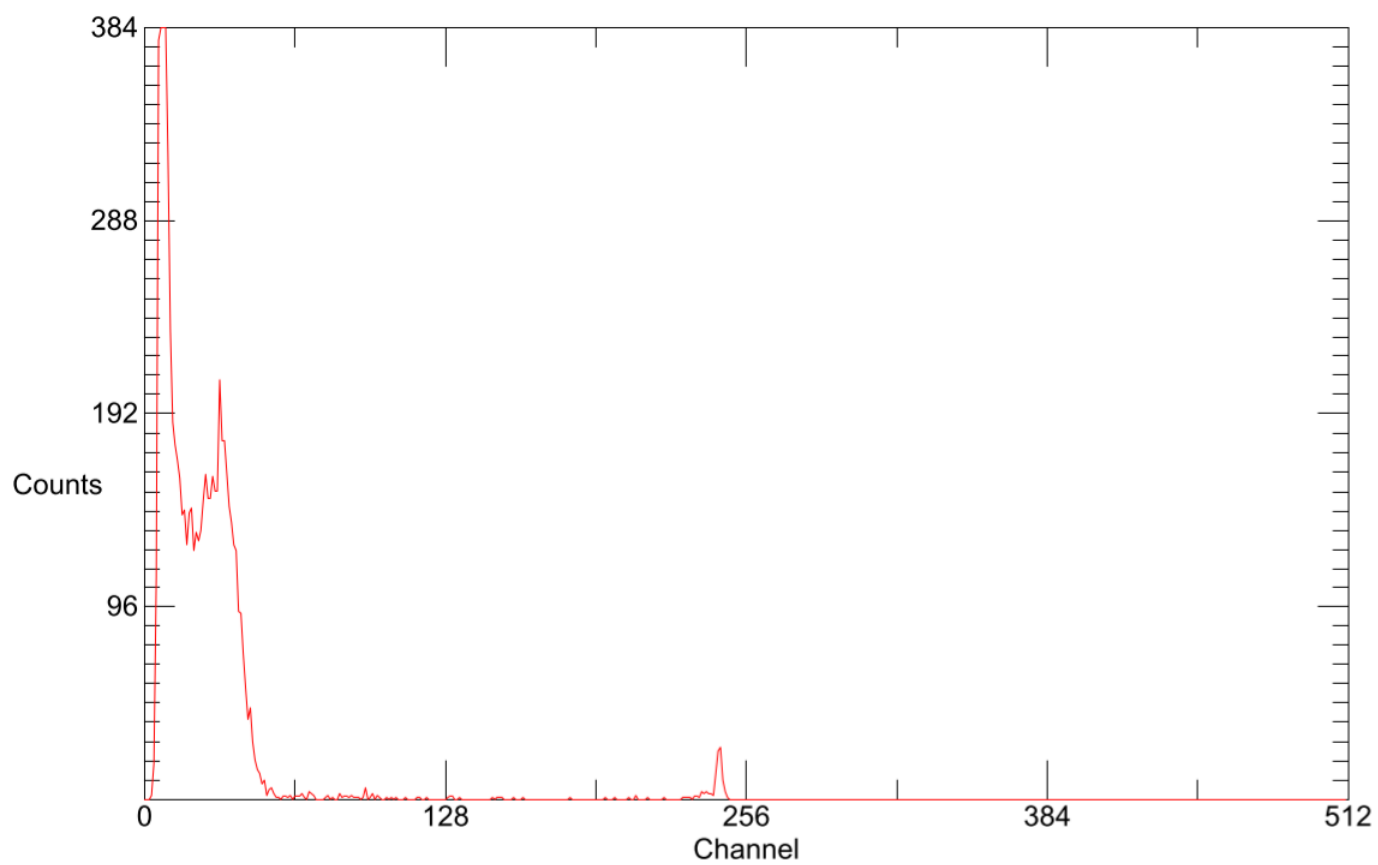


Figure 2.2 Electron spectrum generated for Cesium 137

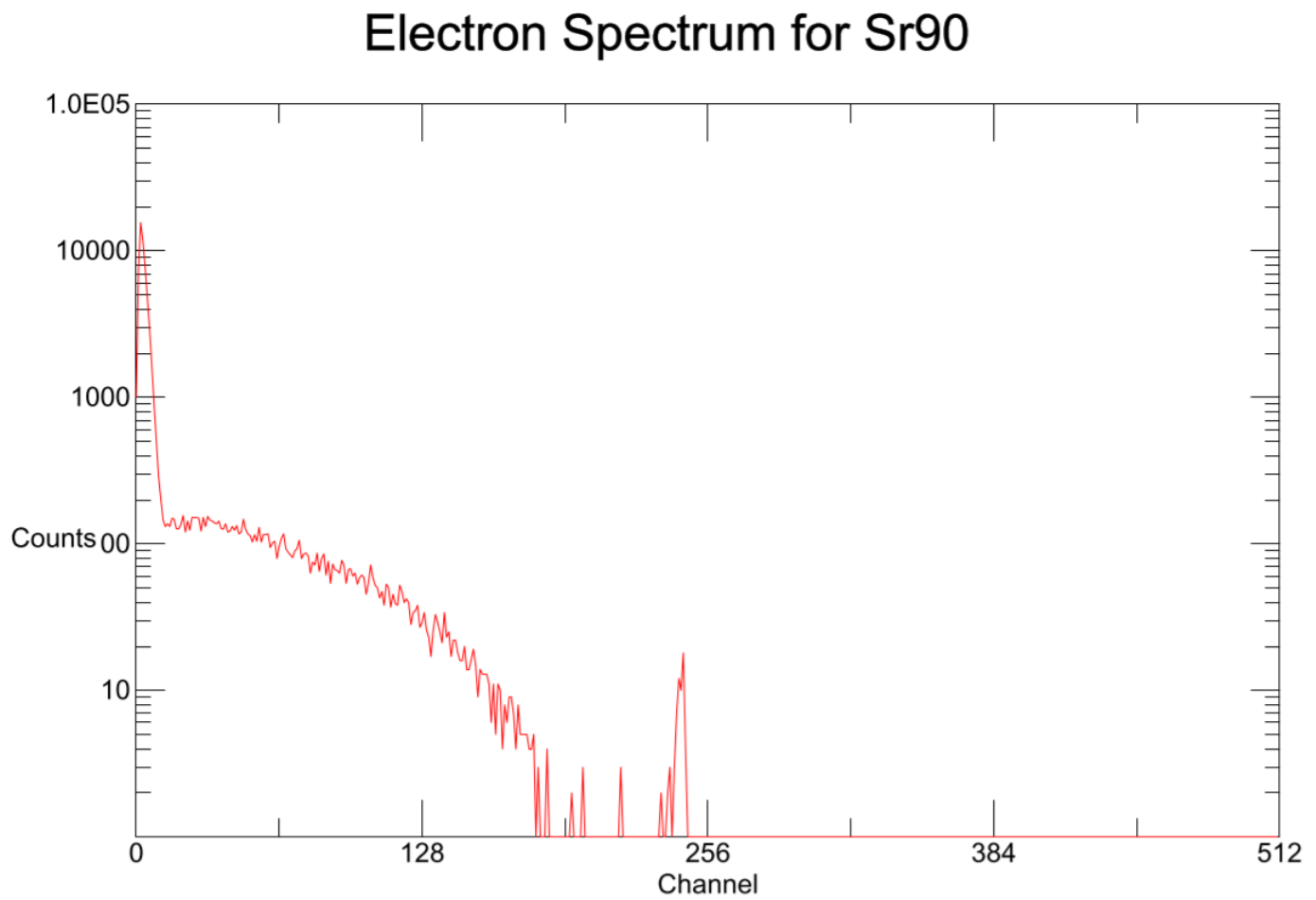


Figure 2.3 Electron spectrum generated for Strontium 90

2.3 Geant4

After verifying that our detector can accurately detect electrons in the 0.5 MeV range, the next step was to verify that it could work for electrons in the multi-MeV range, as this is what we would expect to be emitted by hydrogen fusion events. Due to difficulties in creating an electron source like this, it was necessary to first model our detector. With this model we were able to test detector behavior at higher energies before investing in a higher energy electron source.

The model of our detector was created using Geant4 simulation software. We first started by implementing the crucial components of the detector, namely the aluminum box the PVT is housed in, the silicon wafer, and the reflective Mylar wrapping surrounding the PVT [A.3]. Most of these materials are commonly used in detectors, and as such there were predefined properties for them in Geant4. These included optical properties and densities. PVT however, was not included in Geant4's material library. As such, we took steps to approximate its properties.

We contacted Eljen Technology [9], the manufacturer of the PVT we used, and they generously provided us with the optical data they collected. This data primarily included indexes of refraction for a number of different wavelengths. Other properties of the PVT, such as scintillation constant, and density were already known. To extrapolate these data points to predict optical data for both shorter and longer wavelength photons, we used the Sellmeier equation. The Sellmeier equation [10] is a formula that relates index of refraction to wavelength for certain materials. The most common form of the equation is expressed as such.

$$n^2(\lambda) = 1 + \sum_i \frac{B_i}{\lambda^2/\lambda^2 - C_i}$$

In the Sellmeier formula, $n(\lambda)$ is the index of refraction as a function of wavelength λ . B_i and C_i are two constants that can be experimentally derived. We wrote a script using MATLAB, that took the provided data and approximated the constants B_i and C_i [A.6]. In Fig. 2.4, we plotted the

data provided along with the Sellmeier curve for our approximated indices of refraction. We then used these extrapolated values, along with the density and scintillation constant, to define a custom material in Geant4. The code that defines this custom material can be found in A.4.

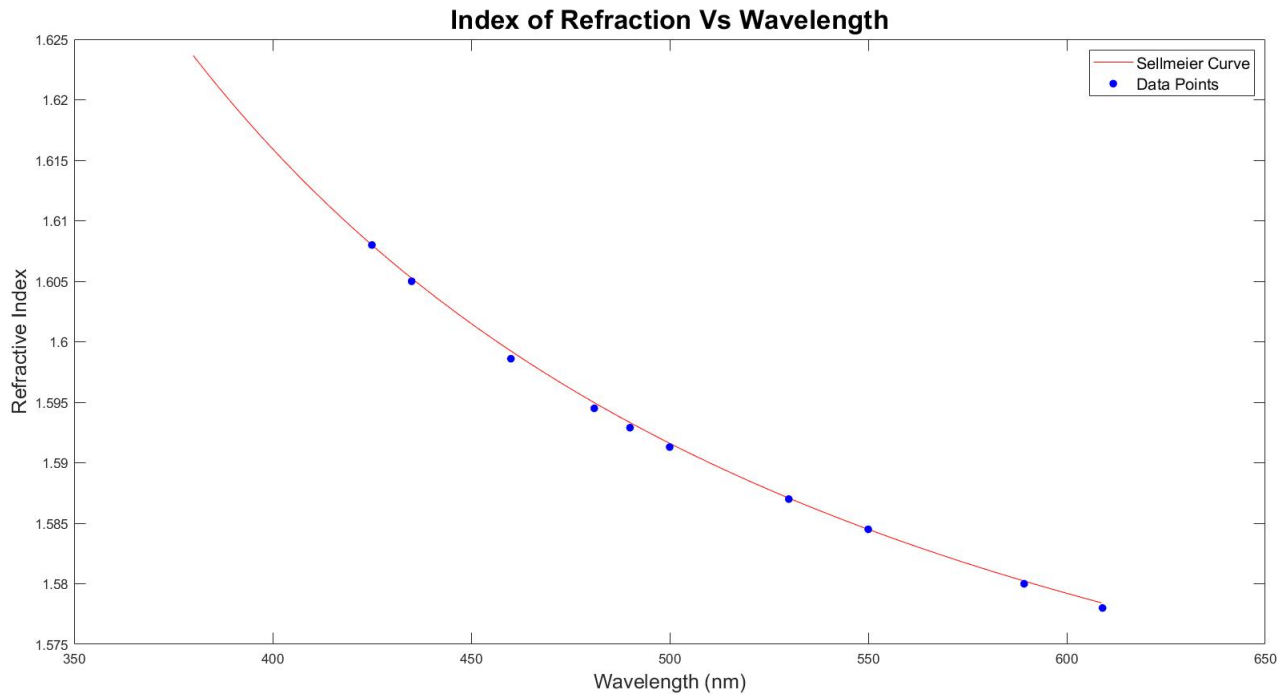


Figure 2.4 Index of refraction vs wavelength for PVT. The curve was derived using the Sellmeier equation, while the data points were provided by the manufacturer of the PVT

We first compared our model to the data we collected on our real detector using Cs 137. Geant4 allows users to define a volume as a sensitive region. When defined as such, Geant4 records how many times the volume was hit, how much energy was deposited by each event, and how many photons passed through the material. We began by defining the polyvinyl toluene as the sensitive region [A.2].

Since Cs 137 emits conversion electrons at 0.625 MeV, we simulated 5 million electrons with this energy hitting our detector. From this simulation we created two key plots [A.5]. The first was a histogram of the energies deposited in our PVT as seen in Fig. 2.5. This plot demonstrated that on

average an electron hitting the PVT deposited about 0.6 MeV. Furthermore, our simulation showed that 93.5% of electrons simulated deposited energy in the PVT.

Figure 2.6 is a histogram of the photon energies generated in the PVT. The first important feature of this plot is that the peaks we generated match those of our Cs137 test as seen in Fig. 2.2. The matching of the peaks indicates that our model is properly simulating the electron spectrum of Cs137. Figure 2.2 does have some additional features from Cs137 β 's that we do not simulate. Furthermore, from this plot can also determine the total number of photons being generated. By dividing the number of photons by the number of electrons we can get an estimated efficiency of our model since this tells us what percentage of results will yield a measurable photon. This was calculated to be 12.6%. From our lab experiments we found that our detector is able to record 8.94% of all electrons that reach our detector. Since it is expected that not all photons will be recorded by our PMTs, the ideal efficiency of our model appears to be in agreement with the actual efficiency of our detector.

However, if a catalyst electron were to be emitted from a deuterium-deuterium fusion reaction, we would expect it to be about 23.5 MeV. We ran our simulation the same as before, but now with the energy of the electrons set to 23.5 MeV. A side view of our detector simulation is shown below in Fig. 2.7. We also made plots of the energy deposited in the PVT, and the energy of the generated photons, as seen in Figs. 2.8 and 2.9.

In addition to determining the wavelength that would be emitted, we calculated the PVT's effectiveness at stopping or slowing electrons. As reported earlier, for 0.625 MeV electrons, 93.469% of the simulated electrons deposited energy in the PVT. However, for the 23.5 MeV electrons, 99.997% of electrons deposited energy in the PVT. Furthermore, with the lower energy electrons we saw a scarcity of photons as only 12.6% of electron events generated a photon. However, with the 23.5 MeV electrons we see a multiplicity of photons, with each electron event on average generating 12.98 photons.

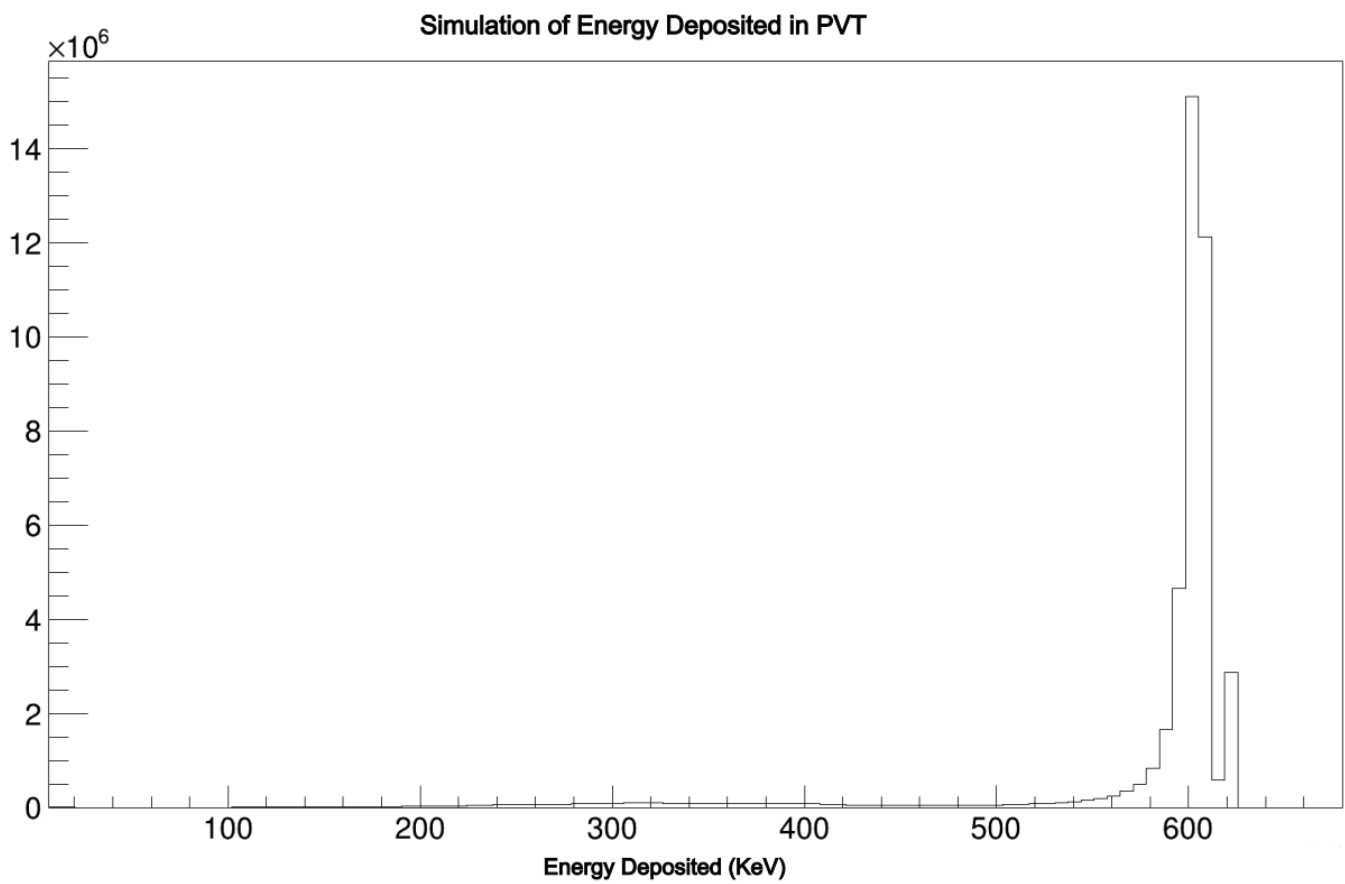


Figure 2.5 Simulated electron spectrum for Cs 137 conversion electrons. The peak around 600 corresponds to 600 KeV. This simulation recorded energy deposited in PVT

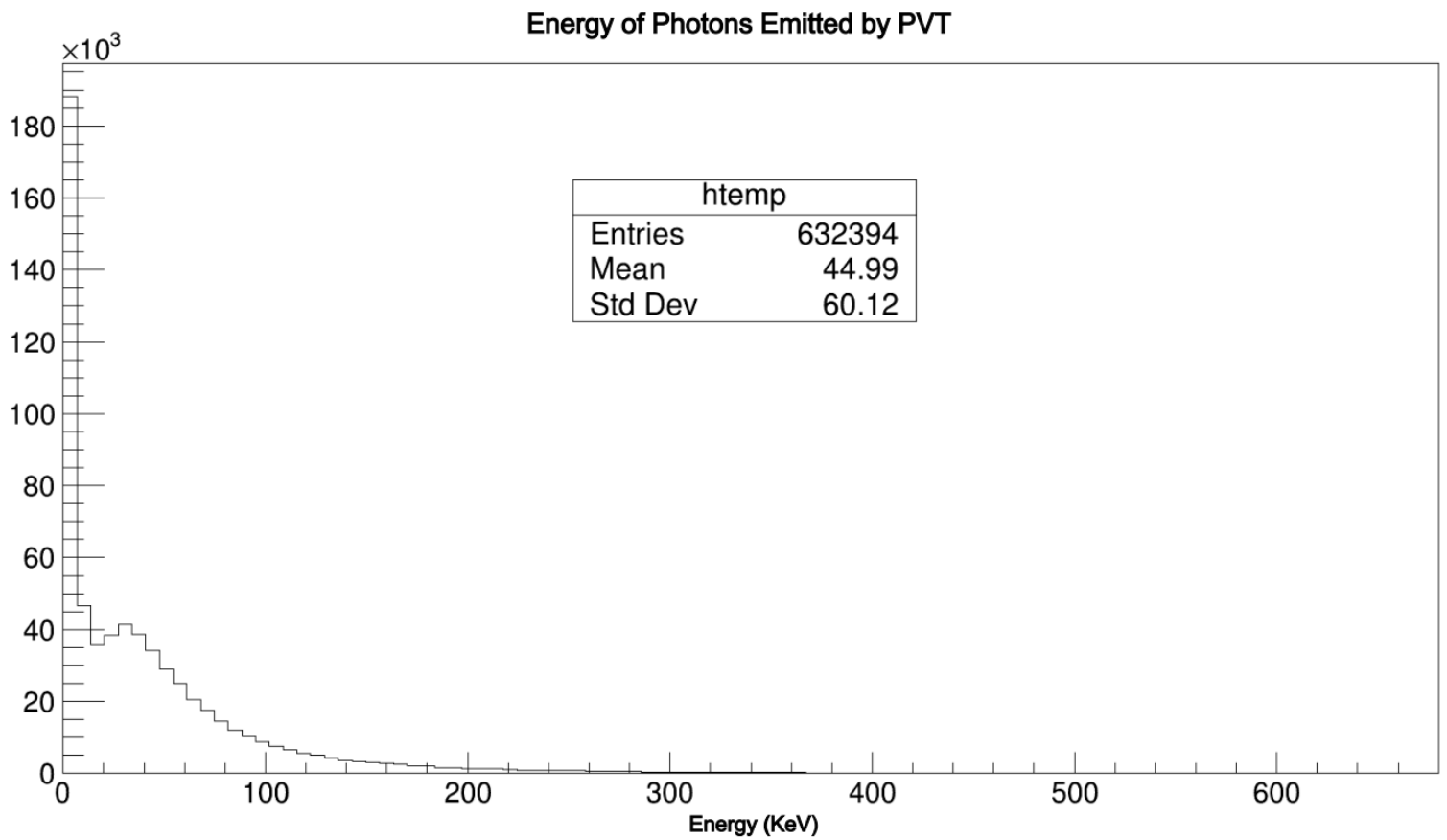


Figure 2.6 This is a histogram of the energy of photons generated by electrons being stopped by the PVT

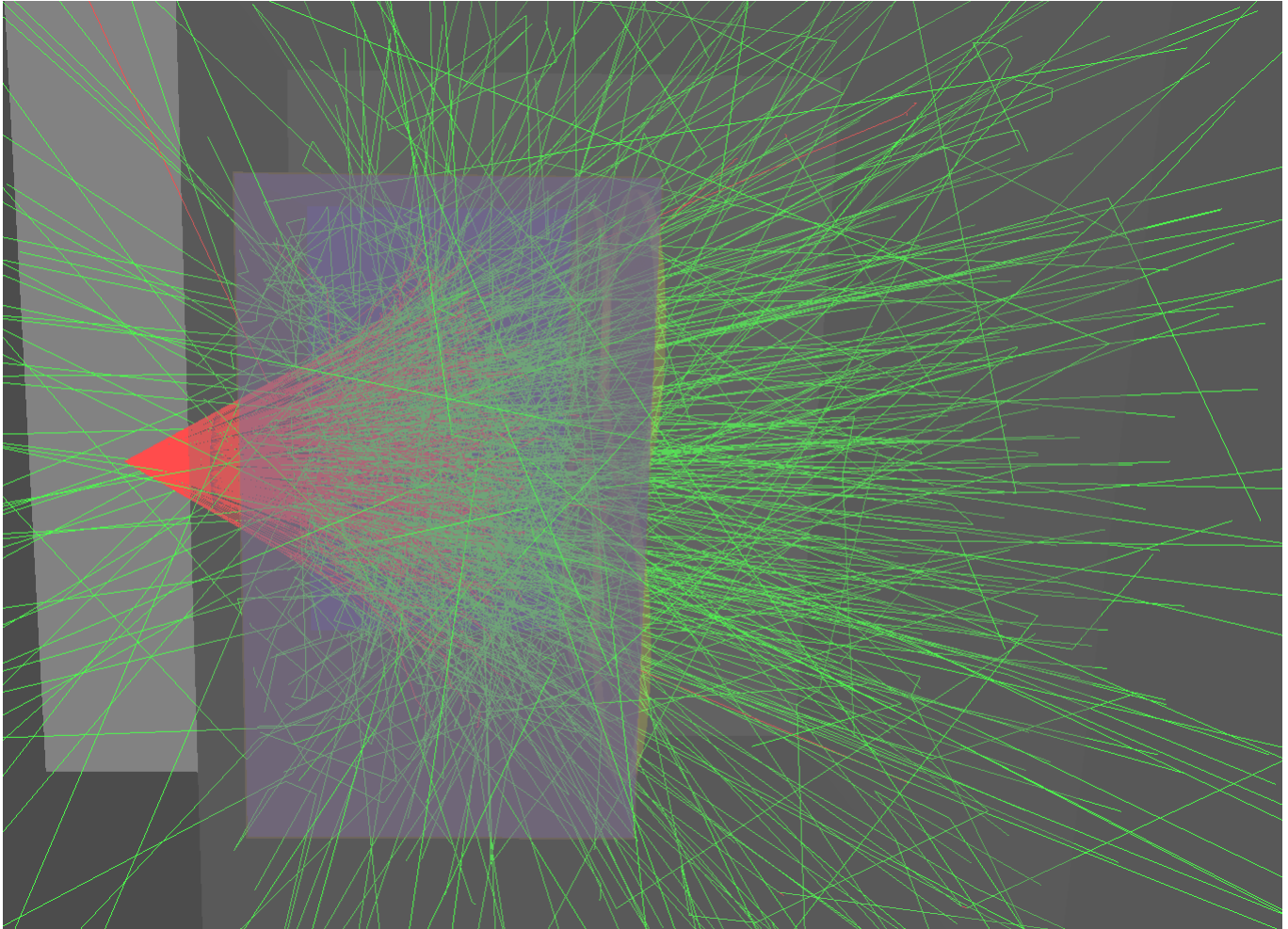


Figure 2.7 Detector Simulation with high energy electrons (23.5 Mev). Red lines are electron paths, with green being the electromagnetic radiation they emit.

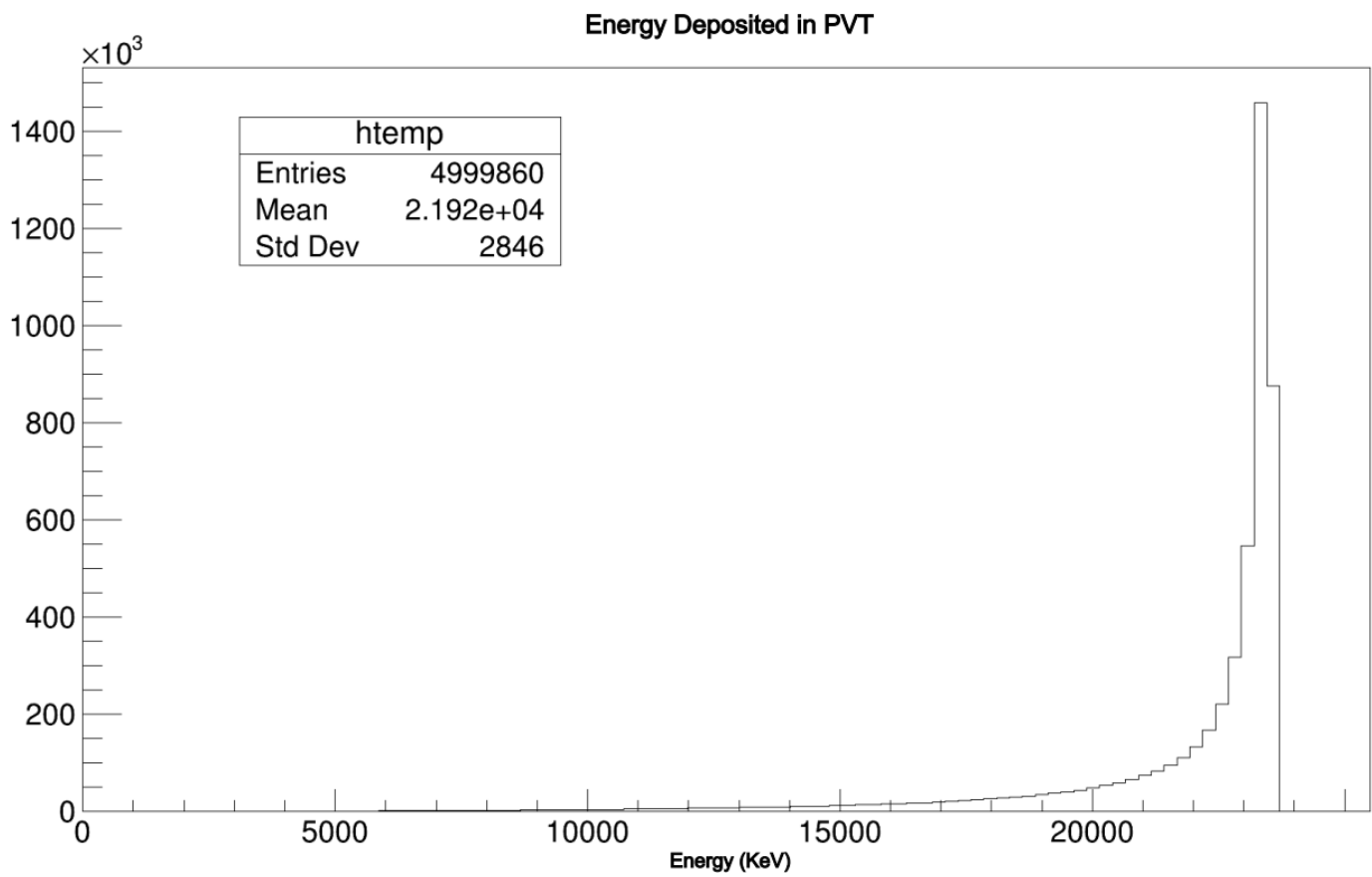


Figure 2.8 Simulated electron spectrum with high energy electrons (23.5 Mev). These are the energies deposited in the PVT.

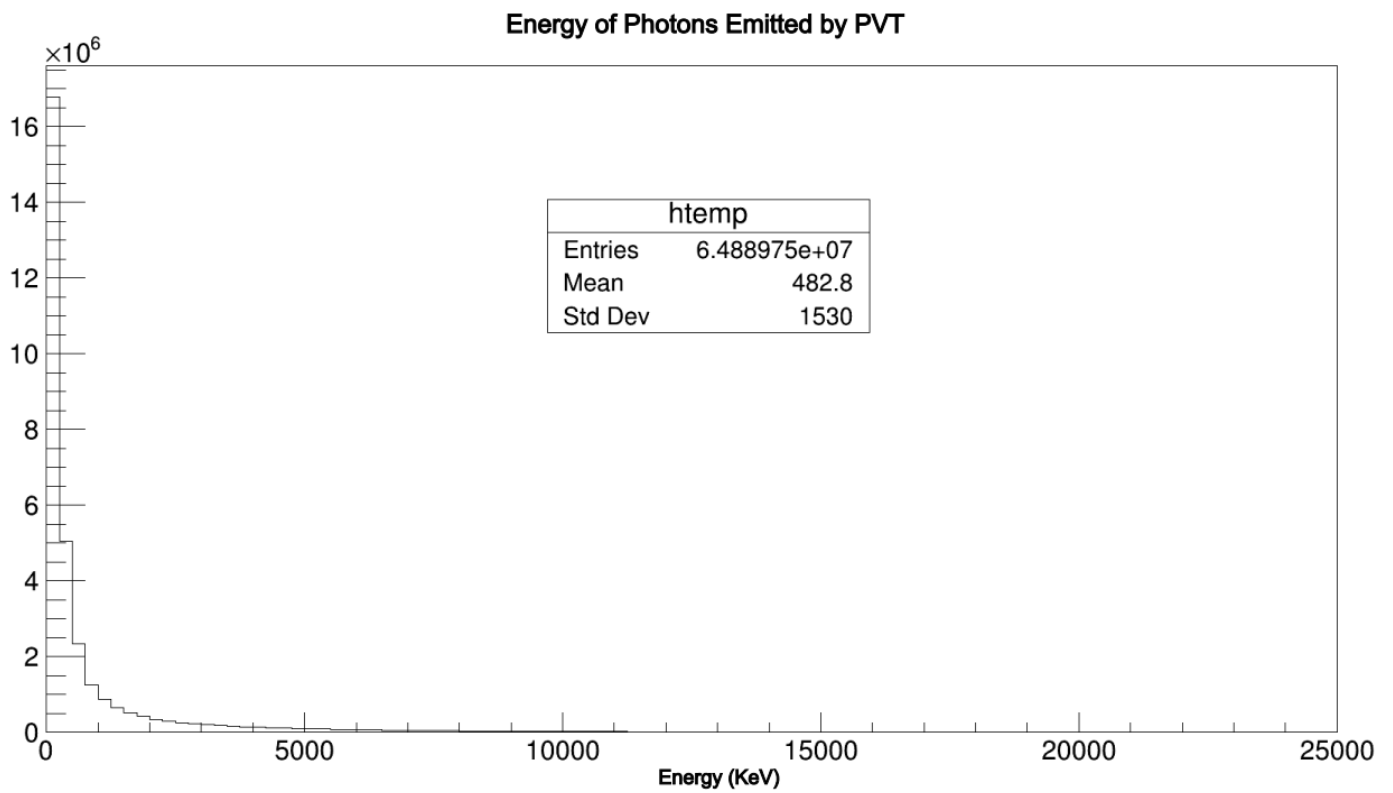


Figure 2.9 Histogram of the energies of photons created by 23.5 MeV electrons being stopped by the PVT

Chapter 3

Results & Conclusions

We started by testing our detector with both Cs 137 and Sr 90 as our electron sources. Both sources were tested in a vacuum, and electron spectrum plots were made for both (Figs. 2.2 & 2.3). As shown, the peaks of our electron spectrum plots match those of other experiments [11]. This demonstrates that our detector is able to detect electrons in the 0.5 MeV range, and it is sensitive enough to pick up the features of the electron's spectrum.

A model was then made using Geant4 particle simulation software. To test our model's efficacy, we ran simulations that would allow us to compare our results to that of our Cs 137 test. We tested this model by bombarding it with 0.625 MeV electrons, the energy of conversion electrons associated with Cs 137 Beta decay. We created an electron spectrum plot as before (Fig. 2.5), and calculated the energies of the photons that were emitted (Fig. 2.6).

The simulations for lower energy electrons match our Cs137 experiments on our detector. Our two spectrum plots (Figs. 2.2 & 2.6) have peaks that match, showing that our simulation is working properly. Furthermore, our simulation has an efficiency that roughly matches our real world experiments demonstrating that our model is being properly simulated.

After this calibration test, the model was then tested with electrons at 23.5 MeV. This is the expected electron energy from a deuterium + deuterium fusion reaction. We chose this for our

simulation since it was the highest energy electron that could be produced from a fusion reaction. With electrons at this energy range, our simulation predicts that our PVT would stop 99.997% of electrons that reach it. Furthermore, each electron that hits it would on average generate 12.98 photons. From the work of previous students, we know that this PVT effectively scintillates for photons up to 9 MeV. Our simulation predicts that the majority of our generated photons would be below this threshold, meaning that this detector would potentially work for electrons in the multi-MeV range. If this is the case, then our detector could be used to detect catalyst electrons emitted from fusion reactions.

Chapter 4

Future Work

There are still some imperfections with our model that need to be resolved. Our simulations for 0.625 MeV electrons show that the PVT is being simulated properly. However, the model is not providing the needed resolution for lower energy photons. This means that at this time we do not know what the lower end of the photon energy spectrum looks like. With better resolution we could better predict detector efficiency, because we could better predict how many photons will have too low of an energy level for our PVT to scintillate.

It is possible however, that these simulation improvements show that this detector design is too inefficient for high energy electrons. If that is the case, then a different detector design may be needed. A more efficient design could be one that does not have to stop the electron in order to collect data. A time of flight detector is a potential solution to this issue. Instead of stopping the electron, this detector would have two small detectors (similar to the Si wafer in ours) that an electron could pass through. The energy of the electron could then be derived by recording the time it takes to travel between the two detectors. For future research in this area, it may be necessary to experiment with a detector design such as this one, especially since its efficiency would be less dependent on electron energy.

Appendix A

Appendix Title

A.1 Electron Spectrum Code

MATLAB code used to process detector data, and create electron spectrum plots

```
1  function plotTotalEvsCount(dir, files, metadata)
2
3  % plot E vs delta E
4
5  channelsEnabled = metadata.channelsEnabled;
6  maxEventsPerFile = metadata.maxEventsPerFile;
7  numEvents = metadata.samplesPerEventPerChannel;
8  CF = metadata.covernionFactor;
9  LtoH = metadata.LowgainToHighgain;
10
11 fileCount = length(files);
12 numClips = 0;
13
14 % get starting point from user
15 jstart = input('\nWhich file do you want to start with? ');
16 istart = input('Which event? ');
17 fprintf('Any key to continue\nCntrl-c to quit\n');
18
```

Figure A.1

```
19 | % loop through the files
20 - | for j = jstart : fileCount
21 |
22 - |     dataFileName = [dir, '/', char(files(j))];
23 - |     fid = fopen(dataFileName, 'r');
24 |
25 |     % loop through the events
26 - |     if j==5
27 - |         totalEvents = 9968;
28 - |     else
29 - |         totalEvents = 10000;
30 - |     end
31 |
32 - |     for i = istart : totalEvents %Find working value for numEvents!!!
33 |
34 |         % skip to selected event
35 - |         if j == jstart && i == istart
36 - |             for k = 1 : istart - 1
37 - |                 Normalize(fid, metadata);
38 - |             end
39 - |         end
40 |         %use to plot vector E vs Cout. E was peaks from waveforms(:,1)
41 |         %was hist(E,130)
42 |         %Originally E was from first channel and deltaE from Channel 3
43 - |         waveforms = Normalize(fid, metadata);
44 |         %peak_DeltaE = max(waveforms.waveforms(:,1));
45 |         %peak_Low_Gain = max(waveforms.waveforms(:,2));
46 |         %peak_High_gain = max(waveforms.waveforms(:,3));
47 |
48 |         %if waveforms.waveforms(1,1) != -1
49 - |             peak_High_gain = max(waveforms.waveforms(:,3));
50 - |             Full_Width(end + 1) = waveforms.waveforms(2,1);
51 - |             Full_Width_Ch2(end + 1) = waveforms.waveforms(3,1);
52 - |             High_Gain(end + 1) = peak_High_gain;
53 |
54 |
55 - |     end
56 - |     close all
57 - | end
58 |
```

Figure A.2

```
59 -     figure(1)
60 -     hist(Full_Width, 50000)
61 -     ylabelStr = ['Count'];
62 -     ylabel(ylabelStr)
63 -     xlabelStr = ['Channel (CH1 Low Gain FWHM)'];
64 -     xlabel(xlabelStr)
65 -     axis([0,512])
66
67 -     figure(2)
68 -     hist(High_Gain, 10000) %was 130
69 -     ylabelStr = ['Count'];
70 -     ylabel(ylabelStr)
71 -     xlabelStr = ['Channel (CH2 High Gain)'];
72 -     xlabel(xlabelStr)
73
74 -     figure(3)
75 -     hist(Full_Width_Ch2, 50000) %was 130
76 -     ylabelStr = ['Count'];
77 -     ylabel(ylabelStr)
78 -     xlabelStr = ['Channel (CH2 High Gain FWHM)'];
79 -     xlabel(xlabelStr)
80
81 -     fclose(fid);
82 - end
```

Figure A.3

A.2 Geant4 Macro File

Macro file used to run Geant4 simulation

```

##using wr1

##      Process class                Model class                Process name
## G4eIonisation                    G4LivermoreIonisationModel    10eV    100GeV    eIoni
## G4eBremsstrahlung                G4LivermoreBremsstrahlungModel 10eV    100GeV    eBrem

/geometry/source HollowBox.tg ##PVTEnergyDep.tg ##pVT10L.tg ##HollowBox.tg

# add physics lists
/physics_lists/select QGSP_BERT_HP_EMV
#cmd below is available only after the cmd above is used
/physics_lists/factory/addRadioactiveDecay

# based on Geant4 example OpNovice2 (EMZ: option4 of EM)
/physics_lists/select QGSC_BERT_EMZ
# cmd below becomes available only when the cmd above is used
/physics_lists/factory/addOptical

/run/initialize

/vis/ASCIITree/verbose 0 #13
/vis/drawTree
#Runs through geometry first to ensure no overlapping volumes or other issues
/geometry/test/run

# Macro test2.g4mac
/control/verbose 0
/tracking/verbose 0
# turn on data recording
/analysis/setFileName ESPECHighE.root          #ESpec.root          #ESPECHighE.root
/event/verbose 0
/gps/verbose 0
/gps/particle e-
/gps/pos/type Plane          ##Point, Plane, Beam, Surface, Volume
/gps/pos/shape Circle       ##Circle, Annulus, Ellipse, Square, Rectangle
/gps/pos/centre -5 0 0 cm   ##centre co-ordinates relative to tg file (X,Y,Z)
/gps/direction 0 0 -15 cm
##/gps/pos/halfx 2 cm
##/gps/pos/halfy 2 cm
/gps/pos/radius 1 mm ##20.4 mm
/gps/pos/rot1 0 0 1 ## not needed to be unit vectors
/gps/position 0 0 15 cm
##/gps/ang/type cos
##/gps/ene/type Lin

#Optional arguments to emit electrons in energy range, instead of at a single energy
#/gps/ene/min .5 MeV
#/gps/ene/max 24 MeV

# energy of electrons we tested
/gps/energy 23.5 MeV #0.625 for CE for Cs137 #23.5 MeV for fusion
/gps/ene/gradient 1
/gps/ene/intercept 1

```

Figure A.4

```
# isotropically emit e-
/gps/ang/type iso
/gps/ang/mintheta 330 deg #-16.52 deg
/gps/ang/maxtheta 360 deg #16.52 deg
/gps/ang/minphi 0 deg #-16.52 deg
/gps/ang/maxphi 360 deg #16.52 deg

# Creates wr1 visualization file
/vis/open DAWNFILE
/vis/open VRML2FILE
/vis/viewer/zoom 1
/vis/viewer/set/background white !! 0
/vis/drawVolume
/vis/scene/add/trajectories
/vis/scene/endOfEventAction accumulate

#Number of electrons simulated
/run/beamOn 5000000 ##300 ##5000000

##Particle Species      Color
##      gamma      green
##      e-         red
##      e+         blue
##      pi+        magenta
##      proton     cyan
##      neutron    yellow
#      other       gray
```

Figure A.5

A.3 Geant4 Geometry File

Geometry file of detector for Geant4 Simulation

```
// for syntax see textgeom.txt, GEANT4 GEOMETRY FROM TEXT FILE version 1.0.
//Default unit is milimeters

:Elem Aluminum Al 13 27
:Mate Aluminum 13 27 2.7

// optical properties of Teflon|
:prop G4_TEFLON
  photon_energies 2 2.5*eV 5.0*eV
  RINDEX 1.36 1.36

:volu theDark BOX 300 300 300 G4_Galactic //G4_AIR //

:rotm r000 0 0 0
  // Rotation matrix: Angle of rotation around global X axis,
  //Angle of rotation around global Y axis,
  //Angle of rotation around global Z axis

:solid block BOX 125 125 75
:solid block2 BOX 125 125 75
:solid wrapper BOX 125.5 125.5 75.5

//Boolean solid for Aluminum box
:solid box1 BOX 150.8125 202.7543 160.3375
:solid box2 BOX 144.4625 152.0114 147.6375
:solid box3 BOX 100.0125 196.4614 147.6375
:solid hollowBox1 SUBTRACTION box1 box2 r000 0 0 0
:solid hollowBox2 SUBTRACTION hollowBox1 box3 r000 0 0 0

//Boolean solid for front plate
:solid front BOX 88.9 120.65 12.7
:solid waferHole TUBE 0 25 25.4
:solid frontPlate SUBTRACTION front waferHole r000 0 0 0
  //Name, BOX, X Half-length, Y Half-length, Z Half-length

:solid wafer TUBE 0 25 0.032 //was .032 mm thick
:solid disk TUBE 0 62.5 2 //Was 0 62.5 2
:solid hole TUBE 0 62.5 20
:solid plate TUBE 0 44.45 20
:solid circle TUBE 0 57.785 6.35
:solid hollowBox3 SUBTRACTION hollowBox2 circle r000 0 0 153.9875 //160.3375
:solid wrap SUBTRACTION wrapper block2 r000 0 0 0
:solid wrap1 SUBTRACTION wrap hole r000 62.5 62.5 -75
:solid wrap2 SUBTRACTION wrap1 hole r000 -62.5 62.5 -75
:solid wrap3 SUBTRACTION wrap2 hole r000 62.5 -62.5 -75
:solid wrap4 SUBTRACTION wrap3 hole r000 -62.5 -62.5 -75
:solid wrap5 SUBTRACTION wrap4 plate r000 0 0 75
  //Name, TUBE, Inner radius, Outer radius, Half length in z
```

Figure A.6

```

//Define materials for each solid
//(s) indicates if that surface is sensitive. Energy deposited in that surface is then recorded
:volu scintillator block G4_PLASTIC_SC_VINYLTOLUENE
:volu Teflon wrap5 G4_TEFLON
:volu SiSBD wafer G4_Si
:volu PMT(S) disk G4_SILICON_DIOXIDE //Was G4_SILICON_DIOXIDE
:volu Window plate G4_PLASTIC_SC_VINYLTOLUENE
:volu aluminumBox hollowBox3 Aluminum
:volu frontPlateAl frontPlate Aluminum
    //Volume name
    //Solid name
    //Material name - From G4NistMaterialBuilder.cc

:place scintillator 1 theDark r000 0 0 0
:place Teflon 1 theDark r000 0 0 0
:place aluminumBox 1 theDark r000 0 0 -72.1375 //-72.6375
:place SiSBD 1 theDark r000 0 0 105
:place PMT(S) 1 theDark r000 62.5 62.5 -77 //Was -77 for all 4 PMT
:place PMT(S) 2 theDark r000 -62.5 62.5 -77
:place PMT(S) 3 theDark r000 62.5 -62.5 -77
:place PMT(S) 4 theDark r000 -62.5 -62.5 -77

// optical properties of the surface between PVT & Teflon
:surf PVT2Teflon scintillator:1 Teflon:1
    type dielectric_dielectric
    model unified
    finish ground
    sigma_alpha 0.1
    property photon_energies 10 .1*eV .5*eV 1*eV 2.5*eV 5.0*eV 10*eV 100*eV 1000*eV 10000*eV 1*MeV
    REFLECTIVITY 0.99 0.99 0.99 0.99 0.99 0.99 0.99 0.99 0.99 0.99 // was 0.95

:color scintillator 0 0 0.9
:color Teflon .5 .3 .1
:color SiSBD .9 0 .9
:color PMT(S) .9 .9 0
:color aluminumBox .2 .2 .2
    //Volume name
    //Red color proportion
    //Green color proportion
    //Blue color proportion
    //Transparency

:vis theDark OFF //Visibility, Example: :VIS yoke OFF
    //Volume name
    //ON or TRUE, OFF or FALSE, By default the visibility of all volumes is set to ON

:prop G4_Galactic
    photon_energies 2 2.5*eV 5.0*eV
    RINDEX 1 1

//Optical Properties of SiO2 and PVT
#include SiO2.tg
#include PVTInterp.tg

```

Figure A.7

A.4 Geant4 PVT File

File used to define custom material for PVT

```
:prop G4_PLASTIC_SC_VINYLTOLUENE
SCINTILLATIONYIELD 10.57/keV
RESOLUTIONSCALE 2
SCINTILLATIONTIMECONSTANT1 2.1*ns
SCINTILLATIONTIMECONSTANT2 10*ns
SCINTILLATIONYIELD1 80
SCINTILLATIONYIELD2 20
photon_energies 100 3.2496*eV 3.23017*eV 3.21097*eV 3.19199*eV 3.17325*eV 3.15471*eV 3.1364*eV 3.1183*eV 3.1004*eV 3.08271*eV \
3.06522*eV 3.04792*eV 3.03082*eV 3.01391*eV 2.99719*eV 2.98066*eV 2.9643*eV 2.94812*eV 2.93212*eV 2.91629*eV \
2.90064*eV 2.88514*eV 2.86982*eV 2.85465*eV 2.83965*eV 2.8248*eV 2.81011*eV 2.79556*eV 2.78117*eV 2.76693*eV \
2.75283*eV 2.73887*eV 2.72506*eV 2.71138*eV 2.69784*eV 2.68443*eV 2.67116*eV 2.65802*eV 2.645*eV 2.63212*eV \
2.61935*eV 2.60671*eV 2.5942*eV 2.5818*eV 2.56952*eV 2.55736*eV 2.54531*eV 2.53337*eV 2.52155*eV 2.50983*eV \
2.49822*eV 2.48672*eV 2.47533*eV 2.46404*eV 2.45285*eV 2.44177*eV 2.43078*eV 2.41989*eV 2.4091*eV 2.3984*eV \
2.3878*eV 2.37729*eV 2.36688*eV 2.35655*eV 2.34632*eV 2.33617*eV 2.32611*eV 2.31614*eV 2.30625*eV 2.29645*eV \
2.28673*eV 2.27709*eV 2.26753*eV 2.25805*eV 2.24866*eV 2.23933*eV 2.23009*eV 2.22092*eV 2.21183*eV 2.20281*eV \
2.19386*eV 2.18499*eV 2.17619*eV 2.16746*eV 2.1588*eV 2.1502*eV 2.14168*eV 2.13322*eV 2.12483*eV 2.11651*eV \
2.10825*eV 2.10005*eV 2.09192*eV 2.08385*eV 2.07584*eV 2.0679*eV 2.06001*eV 2.05219*eV 2.04442*eV 2.03671*eV
RINDEX 1.62302 1.62207 1.62115 1.62024 1.61935 1.61848 1.61763 1.6168 1.61598 1.61518 1.61439 1.61362 1.61287 1.61212 1.6114 \
1.61068 1.60998 1.6093 1.60862 1.60796 1.60731 1.60667 1.60605 1.60543 1.60483 1.60423 1.60365 1.60308 1.60252 \
1.60196 1.60142 1.60088 1.60036 1.59984 1.59933 1.59883 1.59834 1.59786 1.59738 1.59692 1.59646 1.596 1.59556 \
1.59512 1.59469 1.59426 1.59384 1.59343 1.59303 1.59263 1.59223 1.59185 1.59146 1.59109 1.59072 1.59035 1.58999 \
1.58964 1.58929 1.58895 1.58861 1.58828 1.58795 1.58762 1.5873 1.58699 1.58667 1.58637 1.58607 1.58577 1.58547 \
1.58518 1.5849 1.58461 1.58434 1.58406 1.58379 1.58352 1.58326 1.583 1.58274 1.58249 1.58224 1.58199 1.58174 \
1.5815 1.58126 1.58103 1.5808 1.58057 1.58034 1.58012 1.5799 1.57968 1.57946 1.57925 1.57904 1.57883 1.57863 1.57843
```

Figure A.8

A.5 Root Commands

Running the Geant4 script generated a root file that we could extract information from. To create a plot of energy deposited in PVT, the root file was opened in a root script, and the following command was used:

$$t \rightarrow Draw("et[1]")$$

et[1] tells root to grab energies deposited in the first sensitive surface, which in this case was the PVT. Similarly, to create a histogram of photon energies, we used the following root command:

$$t \rightarrow Draw("k", "vln == 1 \&\& pdg == 22")$$

k is the vector of energies of all particles, vlm==1 tells it to look at the PVT, and pdg==22 tells it to plot just photons.

A.6 Sellmeier Code

MATLAB code written to approximate two coefficients of Sellmeier equation. This was then used to extrapolate index of refraction of PVT for different wavelengths.

```

1 - syms C1 C2
2 - [solC1,solC2] = solve(sqrt(1 + C1/(1 + C2/(425^2)))==1.608,sqrt(1 + C1/(1 + C2/(550^2)))==1.5845);
3
4 - C1 = 1.411653100199364;
5 - C2 = -19821.80258648103;
6
7 - lambda = 380:.765:609;
8 - RIndex = sqrt(1 + C1./(1 + C2./(lambda.^2)));
9
10 - lambdaData = [425, 435, 460, 481, 490, 500, 530, 550, 589.26, 609];
11 - RIndexData = [1.608, 1.605, 1.5986, 1.5945, 1.5929, 1.5913, 1.5870, 1.5845, 1.58, 1.578];
12
13 - plot(lambda,RIndex, 'red', lambdaData, RIndexData, '.b', 'MarkerSize', 20)
14 - legend('Sellemeier Curve', 'Data Points')
15 - xlabel('Refractive Index')
16 - ylabel('wavelength nm')
17 - title('Index of Refraction as a Function of Wavelength')
18
19 - %Take lambda and convert into eV with equation E = h*c/lambda
20 - h = 6.626*10^-34;
21 - c = 2.9979*10^8;
22 - EnergyEV = zeros(1,length(lambda));
23 - %Only take every 3 data points
24 - Energy = [];
25 - Index = [];
26 - for j = 1:length(EnergyEV)
27 -     %converts nm to m
28 -     wavelength = lambda(j)*10^-9;
29 -     %calculates energy, multiplies by 6.24e18 to convert to eV, and rounds
30 -     %to 5 decimal places
31 -     EnergyEV(j) = round((h*c/wavelength)*6.241509*10^18,5);
32 -     RIndex(j) = round(RIndex(j),5);
33 -     if rem(j,3) == 0
34 -         Energy(end+1) = EnergyEV(j);
35 -         Index(end+1) = RIndex(j);
36 -     end
37 - end
38
39

```

Figure A.9

Bibliography

- [1] A. Cvetinović, M. Lipoglavsek, S. Markelj, and J. Vesić, “Molecular screening in nuclear reactions,” *Physical Review C* **92** (2015).
- [2] U. Greife, F. Gorris, M. Junker, C. Rolfs, and D. Zahnow, “Oppenheimer-Phillips effect and electron screening in d+ d fusion reactions,” *Zeitschrift fur Physik A Hadrons and Nuclei* **351**, 107–112 (1995).
- [3] C. D. V. Siclén and S. E. Jones, “Piezonuclear fusion in isotopic hydrogen molecules,” *Journal of Physics G: Nuclear Physics* **12**, 213 (1986).
- [4] J. Cruz, H. Luís, M. Fonseca, and A. P. Jesus, “Electron screening effects in nuclear reactions: still an unsolved problem,” *Journal of Physics: Conference Series* **337**, 012062 (2012).
- [5] M. Lipoglavšek, S. Markelj, M. Mihovilović, T. Petrovič, S. Štajner, M. Vencelj, and J. Vesić, “Observation of electron emission in the nuclear reaction between protons and deuterons,” *Physics Letters B* **773**, 553–556 (2017).
- [6] C. E. Rolfs, *Cauldrons in the Cosmos* (The University of Chicago Press, 1988).
- [7] K. Rakes, Master’s thesis, Wright-Patterson Air Force Base, Ohio, 2008.
- [8] W. Loveland, D. Morrissey, and G. Seaborg, *Modern Nuclear Chemistry* (John Wiley Sons, Inc., Hoboken, New Jersey, 2006).

- [9] C. Hurlburt, “Eljen Technology,” Available at <https://eljentechnology.com/> (2022/07/19).
- [10] W. Sellmeier, “Ueber die durch die Aetherschwingungen erregten Mitschwingungen der Körpertheilchen und deren Rückwirkung auf die ersteren, besonders zur Erklärung der Dispersion und ihrer Anomalien,” *Annalen der Physik* **223**, 386–403 (1872).
- [11] *Experiments in Nuclear Science AN34*, 3rd ed., EG&G Ortec, Oak Ridge, Tennessee, 1987.

Index

electron cloud, 6

Index

- conversion electron, iii, 15
- coulomb barrier, 2, 3
- electron, 3, 4, 6
- electron cloud, 3
- electron screening, 3, 6
- electron spectrum, 9–13, 17, 23
- fusion, 1, 3
- gamma ray, 4, 6
- Geant4, iii, 6, 9, 14, 15, 23
- neutron, 2, 4
- polyvinyl toluene, 4, 6, 9, 10, 14
- proton, 2–4
- PVT, 15
- quantum tunneling, 2, 3
- strong nuclear force, 2